Completion Energies and Scale

Eitan Sharon, Achi Brandt*, Ronen Basri†
Dept. of Applied Math
The Weizmann Inst. of Science
Rehovot, 76100, Israel

Abstract

The detection of smooth curves in images and their completion over gaps are two important problems in perceptual grouping. In this paper we examine the notion of completion energy and introduce a fast method to compute the most likely completions in images. Specifically, we develop two novel analytic approximations to the curve of least energy. In addition, we introduce a fast numerical method to compute the curve of least energy, and show that our approximations are obtained at early stages of this numerical computation. We then use our newly developed energies to find the most likely completions in images through a generalized summation of induction fields. Since in practice edge elements are obtained by applying filters of certain widths and lengths to the image, we adjust our computation to take these parameters into account. Finally, we show that, due to the smoothness of the kernel of summation, the process of summing induction fields can be run in time that is linear in the number of different edge elements in the image, or in $O(N \log N)$ *where* N *is the number of pixels in the image, using multigrid methods.*

1. Introduction

The smooth completion of fragmented curve segments is a skill of the human visual system that has been demonstrated through many compelling examples. Due to this skill people often are able to perceive the boundaries of objects even in the lack of sufficient contrast or in the presence of occlusions. A number of computational studies have addressed the problem of curve completion in an attempt to both provide a computational theory of the problem and as part of a process of extracting the smooth curves from images. These studies commonly obtain two or more edge elements (also referred to as *edgels*) and find either the most likely completions that connect the elements or the smoothest curves traveling through them. The methods proposed for this problem generally require massive computations, and their results strongly depend on the energy function used to evaluate the curves in the image. It is therefore important to develop methods which simplify the computation involved in these methods while providing results competitive with the existing approaches. Below we present such a method that directly relates to a number of recent studies of completion and curve salience [9, 18, 5, 19, 12, 7] (see also [2, 6, 8, 14, 15]). Along with simplifying the computations proposed in these studies our method also takes into account the size of edge elements, allowing for a proper computation of completion and saliency at different scales.

A number of studies have addressed the problem of determining the smoothest completion between pairs of edge elements [17, 14, 2, 9, 18, 5]. These studies seek to define a functional that, given two edge elements defined by their location and orientation in the image, selects the smoothest curve that connects the two as its minimizing curve. The most common functional is based on the notion of *elastica*, that is, minimizing the total squared curvature of the curve [9]. Scale invariant variations of this functional were introduced in [18, 5]. While the definition of scale-invariant elastica is intuitive, there exists no simple analytic expression to calculate its shape or its energy, and existing numerical computations are orders-of-magnitude too expensive, as will be shown below.

In the first part of this paper we revisit the problem of determining the smoothest completion between pairs of edges and introduce two new analytic approximations to the curve of least energy. The first approximation is obtained by assuming that the deviation of the two input edgels from the straight line connecting them is relatively small. This assumption is valid in most of the examples used to demonstrate perceptual completions in humans and monkeys [10, 11]. We show that under this simplifying assumption the Hermite spline (see, e.g., [13]) provides a good approximation to the curve of least energy and a very good approximation to the least energy itself. We further develop a second expression, which directly involves the

*Research supported in part by Israel Ministry of Science Grant 4135-1-93 and by the Gauss Minerva Center for Scientific Computation.
†Research supported in part by the Unites States-Israel Binational Science Foundation, Grant No. 94-00100.

angles formed by the edgels and the straight line connecting them. The second expression is shown to give extremely accurate approximations to the curve of least energy even when the input edgels deviate significantly from the line connecting them. We then introduce a new, fast numerical method to compute the curve of least energy and show that our analytic approximations are obtained at early stages of this numerical computation.

Several recent studies view the problems of curve completion and salience as follows. Given M edge elements, the space of all curves connecting pairs of elements is examined in an attempt to determine which of these completions is most likely using smoothness and length considerations. For this purpose [7, 19] define an affinity measure between two edge elements that grows with the likelihood of these elements being connected by a curve. By fixing one of the elements and allowing the other element to vary over the entire image an *induction field* representing the affinity values induced by the fixed element on the rest of the image is obtained. The system finds the most likely completions for the M elements by applying a process that includes a summation of the induction fields for all M elements.

In the second part of this paper we use our newly developed completion energies to define an affinity measure that encourages smoothness and penalizes for gap length. We then use the induction fields defined by this affinity measure to solve the problem of finding the most likely completions for M elements. Since in practice edge elements are never dimensionless, because they are usually obtained by applying filters of a certain width and length to the image, we adjust our affinity measure to take these parameters into account. We do so by relating the scale of these filters to the range of curvatures which can be detected by them and to the orientational resolution needed. Finally, we show that our affinity measure is *asymptotically smooth*, and so can be implemented using multigrid methods and run efficiently in time complexity $O(nm)$ (where n is the number of pixels and m is the number of discrete orientations at every pixel).

The paper is divided as follows. In Section 2 we review the notion of elastica and its scale invariant variation. In Section 3 we introduce the two analytic approximations to the curve of least energy. Then, in Section 4 we develop a fast numerical method to compute the curve of least energy and compare it to our analytic approximations. Finally, in Section 5 we construct an affinity measure taking into account the length and width of the edge filters applied to the image. We then discuss a multiscale (multigrid) method for fast summation of induction fields.

2. Elastica

Consider two edge elements e_1, e_2 positioned at $P_1, P_2 \in \mathcal{R}^2$ with directed orientations Ψ_1 and Ψ_2 respectively measured from the right-hand side of the line passing through P_1 and P_2. Below we shall confine ourselves to the case that $\Psi_1, \Psi_2 \in (-\frac{\pi}{2}, \frac{\pi}{2})$. Denote by $r = \|P_2 - P_1\|$, we may conveniently assume that $P_1 = (0,0)$ and $P_2 = (r,0)$. This is illustrated in Fig. 1(a). Let C_{12} denote the set of C^2 curves through e_1 and e_2. Denote such a curve by its orientation representation $\Psi(s)$, where $0 \le s \le L$ is the arclength along the curve. That is, $x(s) = \int_0^s \cos(\Psi(\hat{s}))d\hat{s}$ and $y(s) = \int_0^s \sin(\Psi(\hat{s}))d\hat{s}$. Also denote the curvature of the curve at s by $\kappa(s) = d\Psi(s)/ds$.

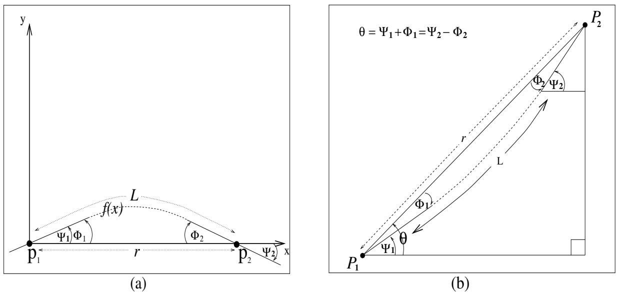

Figure 1. (a) The planar relation between two edge elements, (P_1, Ψ_1) and (P_2, Ψ_2). This relation is governed by $\Phi_1 \in (-\frac{\pi}{2}, \frac{\pi}{2})$, $\Phi_2 \in (-\frac{\pi}{2}, \frac{\pi}{2})$, and r, where Φ_1 and Φ_2 are measured from the line P_1P_2, hence $\Phi_1 = \Psi_1$ and $\Phi_2 = -\Psi_2$. (b) The more general relation between Φ_i and Ψ_i.

The most common functional used to determine the smoothest curve traveling through P_1 and P_2 with respective orientations Ψ_1 and Ψ_2 is the *elastica* functional. Namely, the smoothest curve through e_1 and e_2 is the curve $\Psi(s)$ which minimizes the functional $\Gamma_{el}(\Psi) \stackrel{def}{=} \int_0^L \kappa^2(s)ds$. Elastica was already introduced by Euler. It was first applied to completion by Ullman [17], and its properties were further investigated by Horn [9].

One of the problems with the classical elastica model is that it changes its behavior with a uniform scaling of the image. In fact, according to this model if we increase r, the distance between the two input elements, the energy of the curve connecting them proportionately *decreases*, as can be easily seen by rescaling s (cf. [1]). This is somewhat counter-intuitive since psychophysical and neurobiological evidence suggests that the affinity between a pair of straight elements drops rapidly with the distance between them [11]. Also, the classical elastica does not yield circular arcs to complete cocircular elements. To solve these problems Weiss [18, 5] proposed to modify the elastica model to make it scale invariant. His functional is defined as $\Gamma_{inv}(\Psi) \stackrel{def}{=} L\int_0^L \kappa^2(s)ds$. We believe that a proper adjustment of the completion energy to scale must take into account not only the length of the curve (or equivalently the distance between the input elements), but also the dimensions of the input edge elements. Both the elastica functional and its scale invariant version assume that the input elements have no dimensions. In practice, however, edge elements are frequently obtained by convolving the image with filters of some specified width and length. A proper adjustment of the completion energy as a result of scaling the distance between the elements should also consider whether a corresponding scaling in the width and length of the elements has taken place. Below we first develop useful approximations to the scale invariant functional. (These approximations can also readily be used with slight modifications to the classical elastica measure.) Later, in Section 5, we develop an affinity measure between elements that also takes into account both the distance between the elements and their dimensions.

3. Analytic simplification of Γ_{inv}

Although the definition of both the classical and the scale invariant elastica functionals is fairly intuitive, there is no simple closed-form expression that specifies the energy or the curve shape obtained with these functionals. In this section we introduce two simple, closed-form approximations to these functionals. Our first approximation is valid when the sum of angles $|\Phi_1| + |\Phi_2|$ is relatively small. This assumption represents the intuition that in most psychophysical demonstrations gap completion is perceived when the orientations of the curve portions to be completed are nearly *collinear*. With this assumption we may also restrict for now the range of applicable orientations to $\Psi_1, \Psi_2 \in (-\frac{\pi}{2}, \frac{\pi}{2})$. The second approximation will only assume that $|\Phi_1 - \Phi_2|$ is small, i.e., that the curve portions to be completed are nearly *cocircular*.

Since the curve of least energy is supposed to be very smooth, it is reasonable to assume that within the chosen range of Ψ_1, Ψ_2 the smoothest curve will not wind much. Consequently, it can be described as a function $y = f(x)$, as in Fig. 1(a). Expressing the curvature in terms of x and y we obtain that $\Gamma_{inv}(\Psi) = L\int_0^L \kappa^2(s)ds = L\int_0^r \frac{(f'')^2}{(1+(f')^2)^{\frac{5}{2}}}dx$. For $(\Phi_1, \Phi_2) \to 0$ we get that $L \to r$, and that the variation of $(1 + (f')^2)$ becomes unimportant for the comparison of $\Gamma_{inv}(\Psi)$ over different curves $\Psi \in C_{12}$, so that $\Gamma_{inv}(\Psi) \simeq r\int_0^r (f'')^2 dx$. Hence

$$E_{inv} \stackrel{def}{=} \min_{\Psi \in C_{12}} \Gamma_{inv}(\Psi) \simeq r \min_{\Psi \in C_{12}} \int_0^r (f'')^2 dx \,. \qquad (1)$$

The minimizing curve is the appropriate cubic Hermite spline (see [1])

$$f(x) = x(x - r)\left(\frac{1}{r^2}(t_1 - t_2)x - \frac{t_1}{r}\right) \,, \qquad (2)$$

where $t_1 = \tan\Phi_1$ and $t_2 = \tan\Phi_2$, so that

$$E_{inv} \simeq 4(t_1^2 + t_2^2 - t_1 t_2) \,. \qquad (3)$$

Evidently, this simple approximation to E_{inv} is scale-independent. This leads us to define the scale-invariant *spline* completion energy as: $E_{spln}(\Phi_1, \Phi_2) \stackrel{def}{=} 4(t_1^2 + t_2^2 - t_1 t_2)$. Although the spline energy provides a good approximation to the scale invariant elastica measure for small values of $|\Phi_1| + |\Phi_2|$, the measure diverges for large values. An alternative approximation to E_{inv} can be constructed by noticing that for such small values $\tan\Phi_1 \simeq \Phi_1$ and $\tan\Phi_2 \simeq \Phi_2$. Thus, we may define:

$$E_{ang}(\Phi_1, \Phi_2) \stackrel{def}{=} 4(\Phi_1^2 + \Phi_2^2 - \Phi_1\Phi_2) \,. \qquad (4)$$

We refer to this functional as the scale-invariant *angular* completion energy. This measure does not diverge for large values of $|\Phi_1| + |\Phi_2|$. In fact, when $\Phi_1 = \Phi_2 = \pi/2$ we obtain $E_{ang} = E_{inv} = \pi^2$. In Section 4 below we show that this angular energy is obtained in an early stage of the numeric computation of E_{inv}, and that it provides extremely accurate approximations to the scale invariant least energy functional even for relatively large values of $|\Phi_1|+|\Phi_2|$, especially for small $|\Phi_1 - \Phi_2|$, i.e., for the range of nearly cocircular elements. Using the numeric computation we can also derive the smoothest curve according to E_{ang}:

$$\bar{\Psi}(s) = 3(\Psi_1 + \Psi_2)s^2 - (4\Psi_1 + 2\Psi_2)s + \Psi_1 \,. \qquad (5)$$

The *angular* completion energy can be generalized as follows:

$$E_{gang}(\Phi_1, \Phi_2) = a(\Phi_1^2 + \Phi_2^2) + b(\Phi_1 - \Phi_2)^2 \,, \qquad (6)$$

where Eq. (4) is identical to Eq. (6) with $a = b = 2$. That is, the *angular* completion energy is made of an equal sum of two penalties. One is for the squared difference between Φ_1 and Φ_2, and the other is for the growth in each of them. This suggests a possible generalization of E_{ang} to other weights $a \geq 0$ and $b \geq 0$. One can also think of using energies such as $E_{circ}(\Phi_1, \Phi_2) \stackrel{def}{=} a\Phi_1^2 + b(\Phi_1 - \Phi_2)^2$. A more elaborate study of these types of energies and their properties is presented in [1].

Finally, we note that the new approximations at small angles can also be used to approximate the classical elastica energy, since

$$E_{el} \stackrel{def}{=} \min_{\Psi \in C_{12}} \Gamma_{el}(\Psi) \simeq \frac{1}{r}E_{ang} \simeq \frac{1}{r}E_{spln} \,. \qquad (7)$$

4. Computation of E_{inv}

We use the scale-invariance property of Γ_{inv} in order to reformulate the minimization problem into minimizing over all C_{12} curves of length $L = 1$. (See also [5]). Applying Euler-Lagrange equations (see, e.g., [13]) we get that a necessary condition for $\tilde{\Psi}(\tilde{s})$ to be an extremal curve is that it should satisfy for some λ:

$$2\tilde{\Psi}'' = \lambda\cos\tilde{\Psi} \;\; s.t. \qquad (8)$$
$$\int_0^1 \sin(\tilde{\Psi}(\tilde{s}))d\tilde{s} = 0, \;\; \tilde{\Psi}(0) = \Psi_1, \;\; \tilde{\Psi}(1) = \Psi_2 \,.$$

Considering the very nature of the original minimization problem, and also by repeatedly differentiating both sides of the ODE equation, it can be shown that its solution must be very smooth. Hence, we can well approximate the solution by a polynomial of the form

$$\tilde{\Psi}_n(s) = (1-s)\Psi_1 + s\Psi_2 + s(1-s)\sum_{k=0}^{n} a_k s^k \ , \quad (9)$$

where n is small. (By comparison, the discretization of the same problem presented in [5] is far less efficient, since it does not exploit the infinite smoothness of the solution on the full interval (0,1). As a result the accuracy in [5] is only second order, while here it is "∞-order", i.e., the error decreases *exponentially* in the number of discrete variables n+2 (i.e., $\lambda, a_0, ..., a_n$ from Eq. (8) and (9)).) Fixing n, as well as two other integers $\bar{n}$ and p, we will build the following system of $n+2$ equations for the $n+2$ unknowns $a_0, a_1, ..., a_n, \ and \ \lambda$

$$\tilde{\Psi}''_n(\frac{i+1}{n+2}) + \lambda_n \cos\tilde{\Psi}_n(\frac{i+1}{n+2}) = 0 \ , \ (0 \le i \le n)$$

collocating the ODE, and $\sum_{j=0}^{\bar{n}} w_j \sin\tilde{\Psi}_n(j/\bar{n}) = 0$, where w_j $(0 \le j \le \bar{n})$ are the weights of a p-order numerical integration. Generally, we increase n gradually and increase $\bar{n}$ and p as functions of n in such a way that the discretization error will not be governed by the discretization error of the integration. The nonlinear system of $n+2$ equations is solved by Newton iterations (also called Newton-Raphson; see, e.g. [13].) We start the Newton iterations from a solution previously obtained for a system with a lower n. Actually, only *one* Newton iteration is needed for each value of n if n is not incremented too fast. In this way convergence is extremely fast. At each step, in just several dozen computer operations, the error in solving the differential equation can be *squared*. In fact, due to the smoothness of the solution for the ODE, already for the simple ($n=0, \bar{n}=2$)-system and the Simpson integration rule ($p=3$), a very good approximation to the accurate solution $\tilde{\Psi}(s), \lambda$ and also to E_{inv} is obtained, as can be seen in [1]. The good approximations obtained already for small values of (n,$\bar{n}$) suggest that E_{inv} can be well approximated by simple analytic expressions, as indeed we show in [1] by comparing between several simple approximations to E_{inv}.

Fig. 2 illustrates some of the completions obtained using E_{inv} and the two analytic approximations E_{ang} and E_{spln}. It can be seen that the differences between the three curves is barely noticeable, except in large angles where E_{spln} diverges. Notice especially the close agreement between the curve obtained with the angular energy (Eq. (5)) and that obtained with the scale-invariant elastica measure even in large angles and when the angles deviate significantly from cocircularity.

Note that although the spline curve does not approximate the scale invariant elastica curve for large angles $|\Phi_1|$ and $|\Phi_2|$ it still produces a reasonable completion for the elements. In fact, when the two elements deviate from cocircularity the elastica accumulates high curvature at one of its ends, whereas in the spline curve continues to roughly follow the tangent to the two elements at both ends (see, e.g, Fig. 2(b)) . This behavior is desirable especially when the elements represent long curve segments (see Section 5.2).

5. Completion field summation

Until now we have considered the problem of finding the smoothest completion between pairs of edge elements. A natural generalization of this problem is, given an image from which M edge elements are extracted, find the most likely completions connecting pairs of elements in the image and rank them according to their likelihoods. This problem has recently been investigated in [7, 19]. In these studies affinity measures relating pairs of elements were defined. The measures encourage proximity and smoothness of completion. Using the affinity measures the affinities induced by an element over all other elements in the image (referred to as the *induction field* of the element) are derived. The likelihoods of all possible completions are then computed simultaneously by a process which includes summation of the induction fields for all M elements.

An important issue that was overlooked in previous approaches, however, is the issue of size of the edge elements. Most studies of curve completion assume that the edge elements are dimensionless. In practice, however, edge elements are usually obtained by convolving the image with filters of certain width and length. A proper handling of scale must take these parameters into account. Thus, for example, one may expect that scaling the distance between two elements would not result in a change in the affinity of the two elements if the elements themselves are scaled by the same proportion. Below we first present the general type of *non-scaled* induction underlying previous works. We then modify that induction to properly account for the width and length of the edge elements.

Finally, the process of summing the induction fields may be computationally intensive. Nevertheless, in the third part of this section we show that the summation kernel obtained with our method is very smooth. Thus, the summation of our induction fields can be speeded up considerably using a multigrid algorithm. This result also applies to the summation kernels in [19, 16, 7], and so an efficient implementation of these methods can be obtained with a similar multigrid algorithm.

5.1. Non-scaled induction

In [12, 19] a model for computing the likelihoods of curve completions, referred to as *Stochastic Completion Fields*,

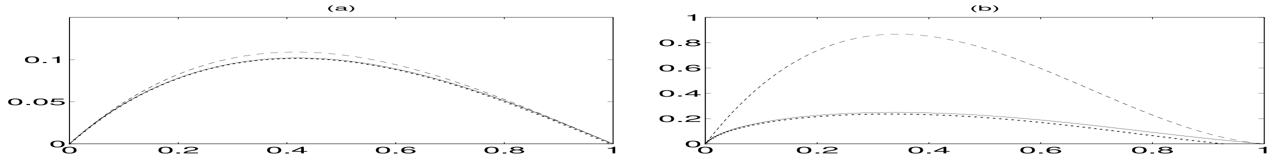

Figure 2. Completion curves: elastica in solid line, $\bar{\Psi}(s)$ (Eq. (5)) in dotted line, and the cubic Hermite spline (Eq. (2)) in dashed line. (a) $\Phi_1 = 30°, \Phi_2 = 15°$, (b) $\Phi_1 = 80°, \Phi_2 = 20°$.

was proposed. According to this model, the edge elements in the image emit particles which follow the trajectories of a Brownian motion. It was shown that the most likely path that a particle may take between a *source* element and a *sink* element is the curve of least energy according to the Elastica energy function[1]. To compute the stochastic completion fields a process of summing the affinity measures representing the source and sink fields was used. In [1] we show, by further analyzing the results in [16], that the affinity measure used for the induction in [19, 16] is of the general type: $A(e_1, e_2) \stackrel{def}{=} e^{-r/r_0} e^{-E_{ang}/(r\sigma_0)}$ (see Fig. 1(b)), where r_0 and σ_0 are strictly positive a-priori set parameters. These parameters need to be adjusted properly according to the scale involved (see Sec. 5.2). Note that for small values of ($|\Phi_1|$,$|\Phi_2|$): $E_{ang}/r \simeq E_{el}$. Hence, $A(e_1, e_2) \simeq e^{-r/r_0} e^{-E_{el}/\sigma_0}$.

Another method which uses summation of induction fields to compute the salience of curves was presented in [7]. In their method the affinity between two edge elements which are cocircular has the form: $e^{-\gamma r} e^{-\delta\kappa}$, where γ and δ are strictly positive constants, κ is the curvature of the circle connecting e_1 and e_2, and r is the distance between e_1 and e_2. A reasonable and straightforward definition in that spirit is $\tilde{A}(e_1, e_2) \stackrel{def}{=} e^{-\gamma r} e^{-\delta E_{spln}}$ where E_{spln} serves as an approximation for E_{inv} according to Eq. (3). Fig. 3 shows an example of computing the "stochastic completion field," suggested by Williams and Jacobs in [19], while replacing their affinity measure with the simple expression $\tilde{A}(e_1, e_2)$. It can be verified by comparing the fields obtained with our affinity measure with the fields presented in [19] that the results are very similar although a much simpler affinity measure was employed.

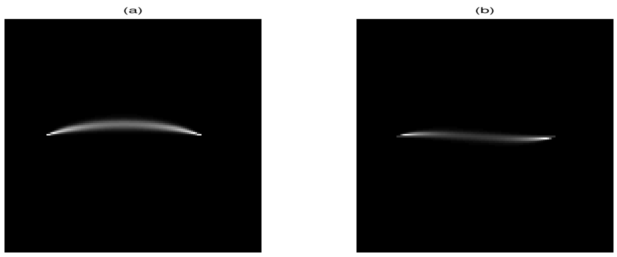

Figure 3. Stochastic completion fields (128 × 128 pixels, 36 orientations) with the induction $e^{-2r} e^{-20E_{spln}}$. (a) $\Phi_1 = 30°$ and $\Phi_2 = 30°$, (b) $\Phi_1 = 30°$ and $\Phi_2 = -30°$. The results closely resemble those obtained in [19].

5.2. Induction and scale

Given an image, an edge element is produced by selecting a filter of a certain length l and width w (e.g., rectangular filters) and convolving the filter with the image at a certain position and orientation. The result of this convolution is a scalar value, referred to as the *response* of the filter. An edge filter may, for example, measure the contrast along its primary axis, in which case its response represents the "edgeness level", or the likelihood of the relevant subarea of the image to contain an edge of (l, w) scale. Similarly, a filter may indicate the existence of fiber-like shapes in the image, in which case its response represents the "fiberness level" of the relevant subarea of the image. Below we use the term "straight responses" to refer to the responses obtained by convolving the image with an edge or a fiber filter.

Consider now the edge elements obtained by convolving the image with a filter of some fixed length l and width w. Every edge element now is positioned at a certain pixel P and is oriented in two opposite directed orientations Ψ and $\Psi + \pi$. The number of edge elements required to faithfully represent the image at this scale depends on l and w. Thus, long and thin elements require finer resolution in orientation than square elements. In fact, the orientational resolution required to sample significantly different orientations increases linearly with l/w (see [4]). Similarly, elements of larger size require less spatial resolution than elements of smaller size. Brandt and Dym ([4]) use these observations in order to introduce a very efficient computation ($O(N \log N)$, where N is the number of pixels in the image) of *all* significantly different edge elements.

Given a particular scale determined by the length l and width w of edge elements, we would like to compute a completion field for this scale. Note that only curves within a relevant range of curvature radii can arouse significant responses for our $l \times w$ elements. Denote the smallest curvature radius that will arouse a still significant response by $\rho = \rho(l, w)$. (Larger curvature radii will arouse significant responses also in larger l/w scales, implying there for a farther-reaching and more orientation-specific continuation.)

By Fig. 4(a) we see that $l/2 = \rho \sin\alpha \approx \rho\alpha$ and $w = \rho - \rho\cos\alpha \approx \rho\alpha^2/2$. Consequently, we have $(l/2\rho)^2 \approx$

[1] Actually, the path minimizes the energy functional $\int_0^L \kappa^2(s)ds + \lambda L$ for some predetermined constant λ.

$\alpha^2 \approx 2w/\rho$, implying that $\rho \approx l^2/8w$.

Next, consider a pair of straight responses. Assuming these elements are roughly cocircular, then, using the relations defined in Fig. 4(b) , the differential relation $\Psi'(s) = 1/\rho(s)$ can be approximated by $(\Psi_1 - \Psi_2)/r \approx 2/(\rho_1 + \rho_2)$, so that $\Omega \approx r/\rho$.

Hence, for completion at a particular scale (l, w), it is reasonable to define for every pair of points P_1 and P_2 a *scale* for the turning angle Ω given by $r/\rho(l, w)$. That is, in the scale (l,w) we define the completion energy between the pair of straight responses so as to depend on the *scaled* turning angle $\Omega\rho/r$. Since $\Omega = \Phi_1 + \Phi_2$, it is straightforward to show that $0.5\Omega \leq \sqrt{E_{ang}(\Phi_1, \Phi_2)} \leq \Omega$. A reasonable definition for the *scaled* angular energy, therefore, is a monotonically decreasing function of $(\rho/r)\sqrt{\Phi_1^2 + \Phi_2^2 - \Phi_1\Phi_2}$.

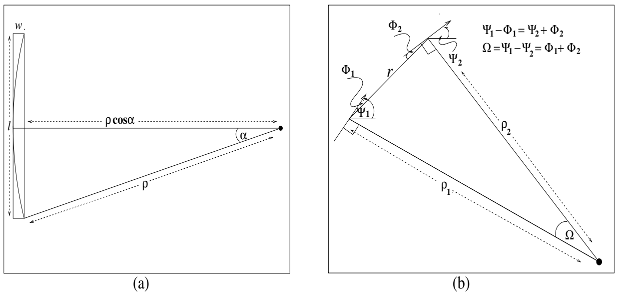

Figure 4. (a) The relation between l,w, and the curvature radius ρ. (b) The turn Ω that a moving particle takes in its way between two straight responses, characterized each by a planar location and an orientation.

Obviously, in any given scale of straight responses, (l, w), for every Φ_1 and Φ_2, the induction of P_1 upon P_2 should decrease with an increase of r/ρ. Hence, we define the field induced by an element e_1 of length l and width w at location P_1 and directed orientation Ψ_1 on a similar element e_2 at (P_2, Ψ_2) by

$$G_{(l,w)}(e_1; e_2) f(u_1) \,, \tag{10}$$

where u_1 denotes the strength of response at e_1, $f(u_1)$ is some appropriate function of this response, and

$$G_{(l,w)}(e_1; e_2) = F_d\left(\frac{r}{\rho}\right) F_t\left(\frac{\rho}{r}\sqrt{\Phi_1^2 + \Phi_2^2 - \Phi_1\Phi_2}\right) . \tag{11}$$

F_d and F_t (the distance and turning attenuation functions, respectively) are smoothly decreasing dimensionless functions that should be determined by further considerations and experience. Thus, our summation kernel is a product of the orientational and the spatial components involved in completing a curve between e_1 and e_2. As we shall see below, this definition has many computational advantages.

Let $\{u_i\}$ denote the set of straight responses for a given scale (l, w), where each u_i is associated with two directed edges $e_i = (P_i, \Psi_i)$ and $\bar{e}_i = (P_i, \Psi_i + \pi)$. The total field induced at any element $e_j = (P_j, \Psi_j)$ by all elements $\{e_i, \bar{e}_i\}$ is expressed by

$$v_j \stackrel{def}{=} \sum_i \left(G_{(l,w)}\left[e_i; e_j\right] + G_{(l,w)}\left[\bar{e}_i; e_j\right]\right) f(u_i) \,. \tag{12}$$

The total field induced at $\bar{e}_j$ by $\{e_i, \bar{e}_i\}$ is given by

$$\bar{v}_j \stackrel{def}{=} \sum_i \left(G_{(l,w)}\left[e_i; \bar{e}_j\right] + G_{(l,w)}\left[\bar{e}_i; \bar{e}_j\right]\right) f(u_i) \,. \tag{13}$$

Since in general the responses obtained by convolving the image with edge filters are bi-directional we may want to combine these two fields into one. This can be done in various ways. The simplest way is to take the sum $\{v_j + \bar{v}_j\}$ as the completion field. Another possibility, in the spirit of [19], is to take the product $\{v_j\bar{v}_j\}$ as the completion field.

Note that the field of a long straight response should be very different (farther-reaching and more orientation-specific) than the sum of the fields of shorter elements composing it, and should strongly depend on its width (see Fig. 5). This suggests that for a comprehensive completion process one must practice a multiscale process, performing a *separate* completion within each scale. The *scaled* induction field (10)-(11), avoids a fundamental difficulty of non-scaled fields like [7, 19, 16]. The latter exhibit so weak a completion for far elements, that it would be completely masked out by local noise and foreign local features.

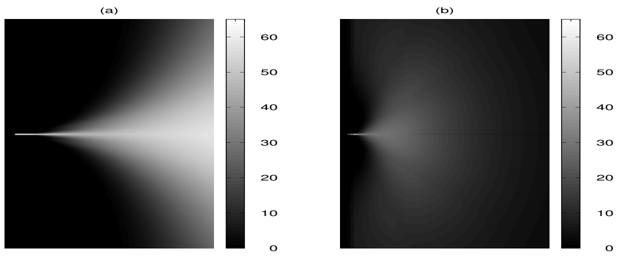

Figure 5. Induction fields (200 $\times$ 200 pixels) in different scales using $F_d(\xi) = e^{-\alpha_1\xi^{\beta_1}}$, and $F_t(\eta) = e^{-\alpha_2\eta^{\beta_2}}$, where $\alpha_1 = 0.5$, β_1=0.5, $\alpha_2 = 128$, and $\beta_2 = 1.5$. (a) The induction field of one long element: $l = 9$, $w = 1/2$, 25 directed orientations. (b) The sum of induction fields of the three shorter elements composing this long element, each consist of: $l = 3$, $w = 1/2$, 12 directed orientations.

5.3. Fast multigrid summation of induction-fields

Let $n = n(l, w)$ be the number of sites (P), and $m = m(l, w)$ the number of orientations (Ψ) at each site, that are required in order to describe all the $l \times w$ straight responses that are significantly different from each other. It can be shown (see [4]) that if l and w are measured in pixel units then, for any N-pixel picture, $n = O(N/lw)$ and $m = O(lN/w)$, so the total number of $l \times w$ elements is $O(N/w)$. Hence, for any geometric sequence of scales (e.g., l=1,2,4,..., and w=1,3,9,...) the total number of straight elements is $O(N \log N)$. It has been shown (in [4]) that all the responses at all these elements can be calculated in only $O(N \log N)$ operations, using a multiscale algorithm that constructs longer-element responses from shorter ones.

At any given scale $l \times w$, it seems that the summations (Eqs. (12) and (13)), summing over $i = 1, 2, ..., nm$ for each value of $j = 1, 2, ..., nm$, would require a total of $O(n^2 m^2)$ operations (even though some of them can be performed in parallel to each other, as in [20]). However, using the smoothness properties of the particular kernel (11), the summation can be reorganized in a multiscale algorithm that totals only $O(nm)$ operations (and the number of unparallelizable steps grows only logarithmically in nm). Indeed, the functions in (11) would usually take on the typical form $F_d(\xi) = e^{-\alpha_1 \xi^{\beta_1}}$, and $F_t(\eta) = e^{-\alpha_2 \eta^{\beta_2}}$. For such choices of the functions, and practically for any other reasonable choice, the kernel $G = G(e_i; e_j) = G(x_i, y_i, \Psi_i; x_j, y_j, \Psi_j)$ has the property of "asymptotic smoothness." By this we mean that any q-order derivative of G with respect to any of its six arguments decays fast with $r_{ij} = \left[(x_i - x_j)^2 + (y_i - y_j)^2\right]^{\frac{1}{2}}$, and the higher q is the faster the decay is. Also, for any fixed r_{ij} (even the smallest, i.e., $r_{ij} = O(l)$), G is a very smooth function of Ψ_i and of Ψ_j.

Due to the asymptotic smoothness, the total contribution to v_j (and $\bar{v}_j$) of all elements *far* from P_j is a smooth function of (x_j, y_j, Ψ_j), hence it need not be computed separately for each j, but can be interpolated (q-order interpolation, with as small an error as desired by using sufficiently high q) from its values at a few representative points. For this and similar reasons, multiscale algorithms, which split the summations into various scales of *farness* (see details in [3]) can perform all the summations in merely $O(nm)$ operations.

6. Conclusion

Important problems in perceptual grouping are the detection of smooth curves in images and their completion over gaps. In this paper we have simplified the computation involved in the process of completion, exploiting the smoothness of the solution to the problem, and have defined affinity measures for completion that take into a proper account the scale of edge elements. In particular, we have introduced new, closed-form approximations for the elastica energy functional and presented a fast numeric method to compute the curve of least energy. In this method the error decreases exponentially with the number of discrete elements. We then have used our approximations to define an affinity measure which takes into account the width and length of the edge elements by considering the range of curvatures that can be detected with corresponding filters of the same scale. Finally, we have shown that solutions to the problem of finding the most likely completions in an image can be implemented using a multigrid algorithm in time that is linear in the number of discrete edge elements in the image. This last observation applies also to recent methods for completion and salience [7, 19]. In the future we intend to use the multigrid algorithm to simultaneously detect completions at different scales in order to combine these completions into a single saliency map.

References

[1] E. Sharon, A. Brandt, and R. Basri, "Completion energies and scale," Forthcoming Technical Report.

[2] M. Brady, W. E. L. Grimson, and D. J. Langridge, "Shape Encoding and Subjective Contours," *Proc. First Annual Conf. Artif. Int.*, 1980.

[3] A. Brandt, "Multilevel computations of integral transforms and particle interactions with oscillatory kernels," *Comp. Phys. Comm.*, **65**:24–38, 1991.

[4] A. Brandt and J. Dym, "Fast computation of multiple line integrals," *SIAM J. Sci. Comp.*, to appear.

[5] A. M. Bruckstein, and A. N. Netravali, "On Minimal Energy Trajectories," *CVGIP*, **49**:283–296, 1990.

[6] S. Grossberg and E. Mingolla, "The Role of Illusory Contours in Visual Segmentation," *The Perception of Illusory Contours*, Petry, S. and Meyer, G. (eds.), Springer-Verlag, New York:116–125, 1987.

[7] G. Guy and G. Medioni, "Inferring Global Perceptual Contours from Local Features," *Proc. DARPA Image Understanding Workshop*:881–892, 1993.

[8] S. Heitger, and Rüdiger von der Heydt, "A Computational Model of Neural Contour Processing: Figure-Ground Segregation and Illusory Contours," *Proc. of ICCV*:32–40, 1993.

[9] B. K. P. Horn, "The Curve of Least Energy," *ACM Trans. on Math. Soft.*, **9**(4):441–460, 1983.

[10] G. Kanizsa, "Organization in Vision," Praeger, New York, 1979.

[11] K. K. Mitesh, L. Minami, D. E. Charles, and W. Gerald, "Improvement in visual sensitivity by changes in local context: Parallel studies in human observers and in V1 of alert monkeys," *Neuron*, **15**:843–856, 1995.

[12] D. Mumford, "Elastica and Computer Vision," *Algebraic Geometry and Its Applications*, Chandrajit Bajaj (ed.), Springer Verlag, pp. 491–506, 1994.

[13] C. E. Pearson (ed.), "Handbook of applied mathematics - Second Edition," Van Nostrand Reinhold Company, New York, 1983.

[14] W. S. Rutkowski, "Shape Completion," *CVGIP*, **9**:89–101, 1979.

[15] A. Sha'ashua and S. Ullman, "Structural Saliency: The Detection of Globally Salient Structures Using a Locally Connected Network," *2nd ICCV*:321–327, 1988,

[16] K. K. Thornber and L. R. Williams, "Analytic Solution of Stochastic Completion Fields," *Biological Cybernetics*, **75**:141–151, 1996.

[17] S. Ullman, "Filling-In the Gaps: The Shape of Subjective Contours and a Model for Their Generation," *Biological Cybernetics*, **25**:1–6, 1976.

[18] I. Weiss, "3D Shape Representation by Contours," *CGVIP*, **41**:80–100, 1988.

[19] L. R. Williams and D. W. Jacobs, "Stochastic Completion Fields: A Neural Model of Illusory Contour Shape and Salience," *ICCV*:408–415, 1995.

[20] L. R. Williams and D. W. Jacobs, "Local Parallel Computation of Stochastic Completion Fields," *CVPR*:161–168, 1996.